

3D Dynamic Finite Element Analysis of the Nonuniform Residual Stress in Ultrasonic Impact Treatment Process

Shengsun Hu, Chaobo Guo, Dongpo Wang, and Zhijiang Wang 

(Submitted January 14, 2016; in revised form May 19, 2016; published online July 11, 2016)

The nonuniform distributions of the residual stress were simulated by a 3D finite element model to analyze the elastic-plastic dynamic ultrasonic impact treatment (UIT) process of multiple impacts on the 2024 aluminum alloy. The evolution of the stress during the impact process was discussed. The successive impacts during the UIT process improve the uniformity of the plastic deformation and decrease the maximum compressive residual stress beneath the former impact indentations. The influences of different controlled parameters, including the initial impact velocity, pin diameter, pin tip, device moving, and offset distances, on the residual stress distributions were analyzed. The influences of the controlled parameters on the residual stress distributions are apparent in the offset direction due to the different surface coverage in different directions. The influences can be used to understand the UIT process and to obtain the desired residual stress by optimizing the controlled parameters.

Keywords finite element model, multiple impacts, nonuniform residual stress, ultrasonic impact treatment, 2024

1. Introduction

The material failure, such as wear, corrosion, and fatigue, is well known to be dependent on the surface state (Ref 1), so many methods have been used to improve the mechanical properties of specimens by inducing compressive residual stress on the surface. Ultrasonic impact treatment (UIT) is a cold-working surface process which is usually employed to produce compressive residual stress by producing plastic deformation. The UIT technology uses high-power ultrasound to produce the vibration of horn and transfer its energy to the impact pins. Due to the high frequency of the system, the surface of the specimen is mechanically peened with a great number of impacts in a short period of time (Ref 2) so that a deeper lay of compressive residual stress can be obtained. The UIT operation is similar to air hammer and shot peening, but the tool is smaller, lighter, and much easier to handle (Ref 3). Due to the advantages, the UIT technology is widely used in the aerospace, automotive, and power plants. Especially in the welding industry, the UIT is used to reduce welding strain, to adjust the residual stress, and to reduce the stress concentration.

Although the mechanical properties of the impacted material have been investigated by many researchers, the dynamic behavior of the material in the impact process is rarely reported. It is difficult to analyze the dynamic behavior by experimental method. With the rapid development of finite element method and of computational power, the multiple dynamic impact

process and the elastic-plastic behavior of the specimen can be evaluated. However, the research works of the finite element analysis now mainly aim at developing an accurate model for the traditional shot peening process. Al-Obaid (Ref 4) firstly established a finite element model using 3D isoparametric solid elements with nine layers through the thickness of the specimen. Subsequently, many types of finite element models were developed to simulate the shot peening process. Mori et al. (Ref 5) established an axisymmetric dynamic viscoplastic finite element model to compute plastic deformation of a circular workpiece with a single shot. Meguid et al. (Ref 6) proposed a novel “symmetric cell” approach to examine the impact effect of a large number of rigid / deformable shots on high-strength steels. Schiffner and Helling (Ref 7) established a 3D model with an equilateral triangle impact surface and three symmetric surfaces to simulate the successive impact process and their influence on the residual stress state. Edberg et al. (Ref 8) developed two 3D models with two symmetric surfaces to analyze the process of a single-shot impact on viscoplastic and elastic-plastic materials. Al-Hassani et al. (Ref 9) developed a 3D finite element model with symmetric surface to simulate single- and five-shot impact to the specimen at different impact velocities and oblique angles. Schwarzer et al. (Ref 10) established a 3D model without symmetric boundary condition to analyze the influence on impact sequence of the shot. With the development of the computation, more and more numerical models were developed to simulate the process of multiple shot impact on the specimen in recent years. Hong et al. (Ref 11) developed a model to investigate the effect of shot diameter, impact velocity, incident angle, and specimen material properties on the residual stress profile, and the relationships of these parameters and the resultant residual stress characteristics can be extended to multiple shot impacts. Majzoubi et al. (Ref 12) developed a 25-shot model for multiple-shot impacts on a specimen at different velocities. The number of shots was up to 134 in the 3D finite element model established by Bagherifard et al. (Ref 13), which aimed at describing and characterizing the surface layer of the specimen. Klemenz et al. (Ref 14) simulated 121-rigid shot impact on the steel material with the same velocity.

Shengsun Hu, Chaobo Guo, Dongpo Wang, and Zhijiang Wang, Tianjin Key Laboratory of Advanced Joining Technology, Tianjin University, Tianjin 300350, China and School of Materials Science and Engineering, Tianjin University, Tianjin 300350, China. Contact e-mail: wangzj@tju.edu.cn.

The UIT can be considered as the further development of shot peening, and they have many aspects in common. For example, the impact process is an elastic-plastic dynamic process in which the specimens are impacted by the hardened materials, and then the compressive residual stress is induced by producing plastic deformation. Therefore, the UIT model could be established by improving the shot peening model. Comparing with the shot peening process, the UIT process has some different characteristics too; for example, the impact pin size is large and the impact velocity is low. Beside this, the large number of impacts in the device moving direction, which is much larger than that in the shot peening process, produces high surface coverage, while in the device offset direction the coverage is smaller. The different coverage in the different directions induces the nonuniform residual stress distributions, which represents the main difference from the shot peening process. Therefore, the shot peening model should be improved to compromise the differences between the two processes.

The paper aims at developing a UIT model with multiple impacts and investigating the residual stress distributions with different controlled parameters. Section 2 introduces the UIT device and presents the numerical model of the UIT process. Section 3 uses the numerical model to simulate the typical UIT process and verifies the numerical model. Section 4 discusses the simulation results. Finally, the conclusions are drawn in section 5.

2. Finite Element Model for the UIT Process

2024 aluminum alloy was processed by the UIT technology in experiments. The chemical composition of 2024 is given in Table 1.

2.1 UIT Device Parameter Settings

The UIT device model used in the following experiments was TJU-HJ-III (Fig. 1(b)), developed by Tianjin University. Its configuration is shown in Fig. 1(a). A typical compressive residual stress induced by the UIT technology in the near-surface region is as shown in Fig. 1(c). The frequency of output ultrasonic vibration is 20 kHz and the amplitude range is 0-25 μm for the UIT device. Single-pin mode was employed and its size is shown in Fig. 2. The diameter of the pin ϕ was 4 mm, the length L was 30 mm, the tip was semi-ellipsoid, and the semi-axis b was 1 mm.

2.2 Finite Element Model of UIT

In the finite element model, the following assumptions were employed:

- (1) The pin is considered as a rigid body and the specimen is considered as nonlinear kinematic hardening material.
- (2) The initial velocity is assumed to be constant during each impact process. The initial velocity of the pin de-

Table 1 Chemical composition of 2024 aluminum alloy (wt.%)

Elements	Cu	Si	Fe	Mn	Mg	Zn	Cr	Ti	Al
2024	3.80-4.90	0.50	0.50	0.30-0.90	1.20-1.80	0.25	0.10	0.15	balance

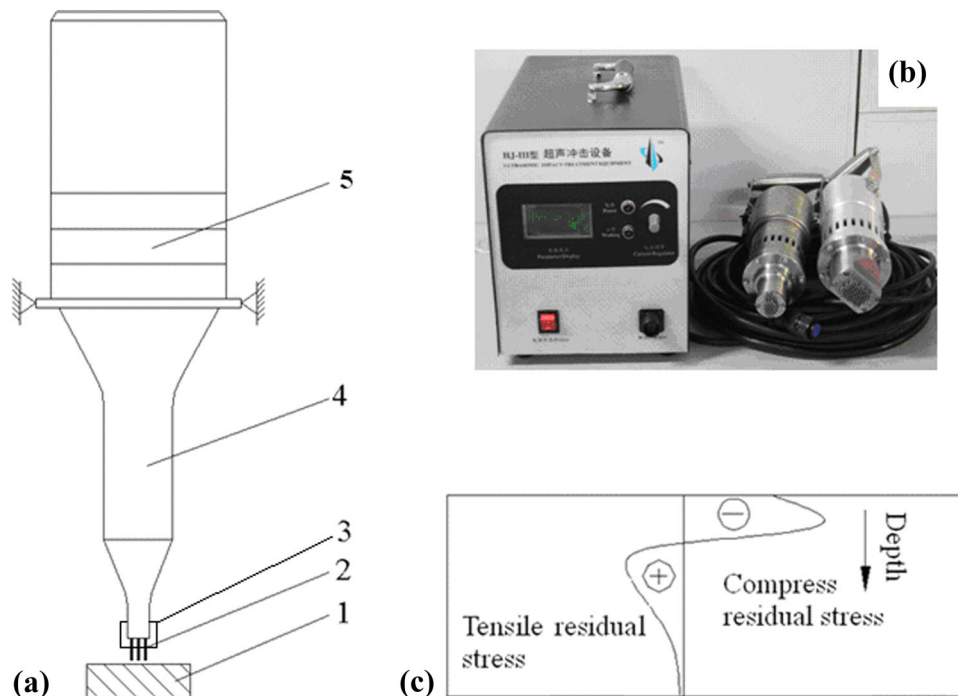


Fig. 1 The UIT device. (a) Device configuration (1. specimen, 2. pins, 3. head body, 4. ultrasonic horn, 5. energy transducer); (b) experimental device; and (c) typical residual stress profile

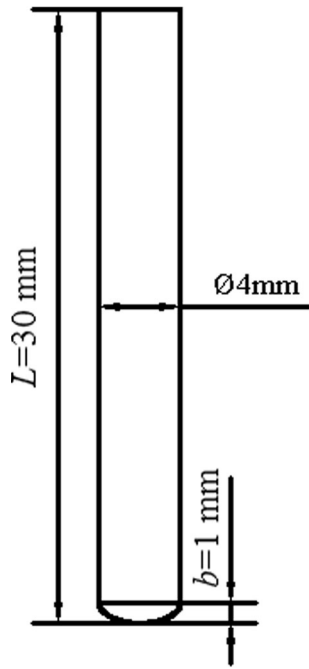


Fig. 2 Geometry and size of the impact pin

depends on the collisions between the ultrasonic horn and the pin. Chaise et al (Ref 15) took the average velocity of the rod as the maximum initial velocity in ultrasonic shot peening process. The maximum initial velocity of the shot is

$$v_{ini\ max} = 2\pi Af. \quad (\text{Eq 1})$$

In this study, the same theory was used to calculate the initial velocity. The vibration frequency f was 20 kHz and the amplitude A was 16 μm . Thus, the velocity $v_{ini\ max}$ was about 2 m/s which was considered as the initial impact velocity.

- (3) The pin impacts on the specimen perpendicularly. In fact, the pin does not impact on the specimen perpendicularly due to the inevitable contacts between the pin and the device head. The contacts and the incident angle (the angle between the pin and the specimen when the pin contacts the specimen) are not predictable. To simplify the impact process simulation, the incident angle of the pin is considered as zero.
- (4) The frequency of output ultrasonic vibration is set as 20 kHz which is the same as the actual parameters. The impact frequency between the pin and the specimen is much lower than the output ultrasonic vibration frequency. Considering the capacity of the UIF device, the impact frequency f_i is considered as 100 Hz.

Using the assumptions above, a finite element model was established by the commercial software package ABAQUS/Explicit, in which the impact zone was restricted to a small region. In practice, the UIT process of the whole or part of the specimen surface should be simulated. But it is an impossible task for the current hardware and simulation software if all the impacts are simulated. Because the distributions of the residual stress cannot be influenced by the other impacts whose distance

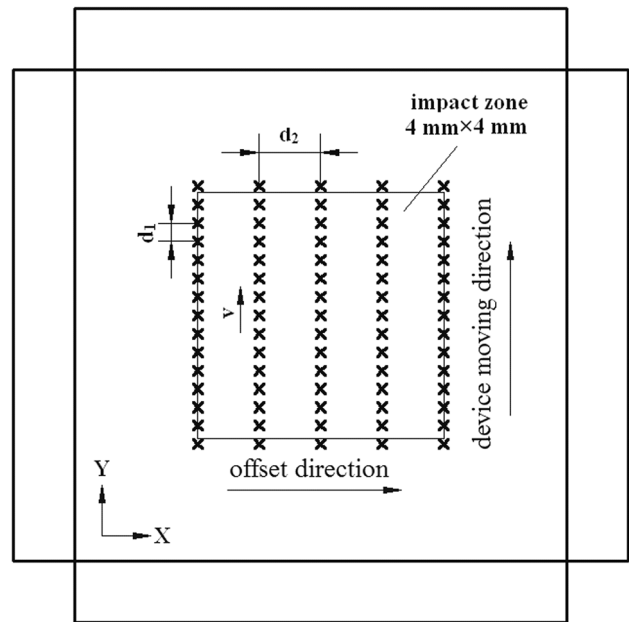


Fig. 3 Impact locations of the pin in multi-impact model

Table 2 Relationship between device traveling velocities and distance between the locations

Device moving velocities v , m/min	Distance between the locations d_1 , mm	Pin number in each row
1.2	0.2	21
1.8	0.3	15
2.4	0.4	11

is more than 2 mm (Ref 16), the impact zone was restricted within 4 mm \times 4 mm, as shown in Fig. 3.

In the model, some parameters are the same as in our previous work (Ref 17). The geometric property of the specimen was 8 mm \times 8 mm \times 5 mm. And the cells of the specimen were hexagonal elements with reduced integration (C3D8R) elements, which is shown in Fig. 4, and the bottom of it was restrained against all displacements. All side faces were surrounded by infinite elements which provide quiet boundaries by minimizing the reflection of dilatational and shear waves back into the region of interest. The pin was modeled according to the actual pin, and it was also meshed with C3D8R elements.

In the impact process, the friction coefficient between the pin and the specimen was assumed to be 0.25. Due to the large deformation, the Johnson-Cook equation, in which both work hardening and strain rate hardening are taken into account, was chosen to evaluate the stress-plastic strain relations. The Johnson-Cook equation is

$$\sigma = [A + B(\epsilon)^n] \left[1 + C \ln \left(\frac{\dot{\epsilon}}{\dot{\epsilon}_0} \right) \right] \left[1 - \left(\frac{T - T_0}{T_m - T} \right)^m \right], \quad (\text{Eq 2})$$

where σ is the stress to be evaluated, $\dot{\epsilon}_0$ and T_0 are, respectively, the reference values of strain rate and temperature, $\dot{\epsilon}$ and T are, respectively, the strain rate and temperature under consideration, T_m is the melting temperature, and A , B , C , m , and n are the material constants to be determined. Due to the small temperature increase in the impact process, the influ-

ence of the temperature is negligible. In this study, the Johnson-Cook properties (Ref 18) were 369 MPa, 684 MPa, 0.0083, 1.7, and 0.73.

The impact process includes several impact rows, and every row consists of successive impacts, as shown in Fig. 3. In each impact row, one pin impacts on the specimen sequentially in the device moving direction. The distance between adjacent locations d_1 is determined by the device moving velocities, and it can be calculated with the following equation:

$$d_1 = \frac{v}{f_i}, \quad (\text{Eq 3})$$

where v denotes the device moving velocities and f_i is the impact frequency. By calculation, the relationship between the velocities v and the distance d_1 is shown in Table 2. After the impacts in the previous row, the new impact row offset a certain distance d_2 in the offset direction. For example, when the moving velocity of the device is 1.8 m/min, the distance between adjacent pins in each row is $d_1 = 0.3$ mm, thus 15 impacts are chosen for each row. When the device offset distance is $d_2 = 1$ mm, 5 rows are in the impact zone.

The influences of the different controlled parameters, including pin velocities, pin sizes, device moving velocities, and device offset distances, on the residual stress distributions were simulated by the model. In the simulation, controlling variable method, which changes a controlled parameter at a time, was employed to analyze the influences.

3. Typical UIT Process Simulation and Model Verification

3.1 Typical UIT Process Simulation

The UIT process consists of multiple impacts. In order to analyze the propagation of the stress in the impact process, the numerical model with only three impacts in one row was developed. The distance between the impact location centers is 0.3 mm. The residual stress fields with the first three impacts are shown in Fig. 5. The residual stress was symmetrical after the first impact. As the prestress for the second impact, the compressive residual stress induced by the first impact is beneficial to increase the compressive residual stress for further impact, due to which the location of the maximum residual stress changes and moves toward the latter impact. The maximum residual stress located between two impacts after the second impact. The second impact increased in the plastic zone, which decreased the nonuniformity of the plastic deformation beneath the first impact indentation. Then the third impact further increases the maximum compressive residual stress of the specimen. The third impact indentation does not overlap the first indentation center, and the zone under the first indentation does not get the extra energy transferred from the third impact, thus the uniformity of the plastic deformation improved by the third impact decreases the maximum compressive residual stress under the first indentation. From the analysis above, it can be deduced that further impacts will move the maximum compressive residual stress in the device moving direction gradually and improve the uniformity of plastic deformation.

However, the distances between the adjacent indentations are different in the two directions, which determine the different effects of the impacts on the residual stress distributions. Fig. 6



Fig. 4 Cells of the numerical model

shows the residual stress fields of the first three impact rows ($d_2 = 1$ mm). Because of the low surface coverage in the device offset direction, the influence of the adjacent indentations on the residual stress is weak and the location of maximum compressive residual stress does not change. But the prestress induced by the former impact row will promote the maximum compressive residual stress induced by the latter impact row to move toward the former impact rows, as shown in Fig. 6(b) and (c). Fig. 7 which show the residual stress field with multiple impacts. Due to the large surface coverage in the device moving direction, the residual stress distribution is more uniform than the that in the offset direction.

3.2 Model Verification

Due to the small impact region in the UIT numerical model, it is not possible to verify the numerical result by performing experimental measurement directly. In this section, the impact region was enlarged to 20 mm × 20 mm, and the specimen size was 100 mm × 100 mm, as shown in Fig. 8. In the experiment, $d_1 = 0.3$ mm and $d_2 = 1$ mm. Due to the nonuniformity, the average residual stress under the center indentation of the specimen surface was measured by experimental x-ray diffraction (XRD), as shown in Fig. 9, to verify the accuracy of the model. The numerical residual stress distribution is in good agreement with the experimental result.

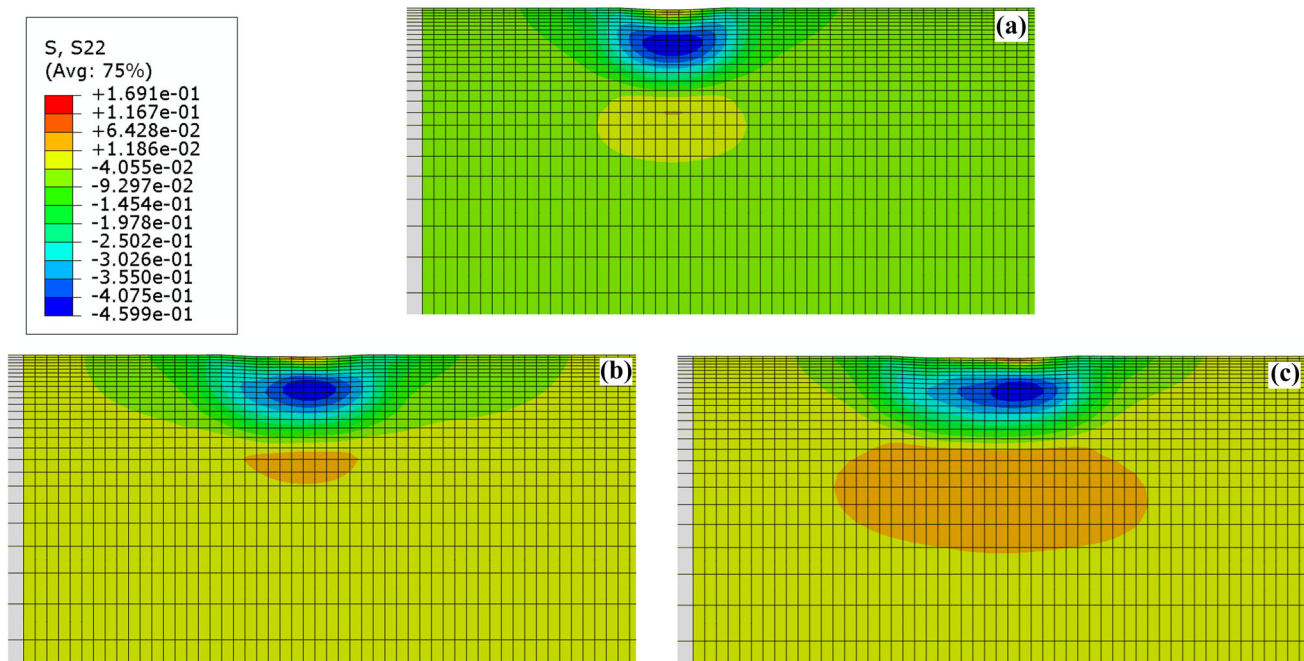


Fig. 5 Residual stress in device offset direction in X - Z plane with different impacts: (a) first impact, (b) second impact, and (c) third impact

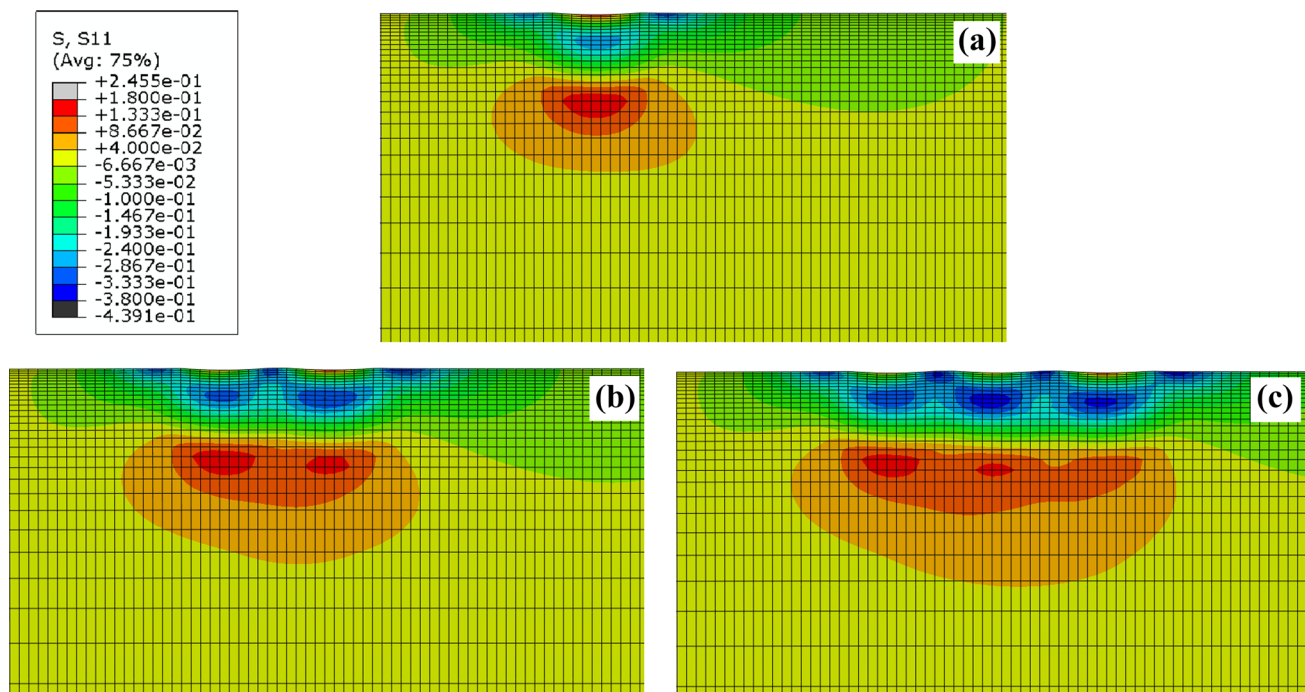


Fig. 6 Residual stress in device moving direction in Y - Z plane with different impacts: (a) one impact row, (b) two impact rows, and (c) three impact rows

4. Influences of Controlled Parameters on Residual Stress Distribution

4.1 Influence of Initial Impact Velocity

From the assumptions of the numerical model, the initial impact velocity of the pin can be varied by modifying the device amplitude. Three different initial velocities (1, 2, and

3 m/s) were considered to analyze the residual stress distributions. The residual stresses with the depth along the center line and the line offset from the center line (the offset distance is 1 mm) in the offset direction were separately obtained, as shown in Fig. 10. The penetration depth increases with the initial velocities attributed to the increase of energy transferred to the specimen. And the nonlinear increase of the penetration depth can be explained by the nonlinearity of the stress-strain curve.

Table 3 Main residual stress parameters with different impact velocities and pin diameters along the center line and offset line

Velocity, m/s	Diameter, mm	Centerline				Offset line			
		$d_b^x, \mu\text{m}$	$\sigma_{\text{max}}^x, \text{MPa}$	$d_b^y, \mu\text{m}$	$\sigma_{\text{max}}^y, \text{MPa}$	$d_b^x, \mu\text{m}$	$\sigma_{\text{max}}^x, \text{MPa}$	$d_b^y, \mu\text{m}$	$\sigma_{\text{max}}^y, \text{MPa}$
2	4	665	378	723	375	651	355*	523	200
3	4	923	354	972	338	875	355	821	316
2	4.9	774	376	839	350	763	325	749	265

d_b^x is the penetration depth in the offset direction, d_b^y is the penetration depth in the device moving direction, σ_{max}^x is the maximum compressive residual stress in the offset direction, σ_{max}^y is the maximum compressive residual stress in the offset direction

* Maximum compressive residual stress appeared at the specimen surface

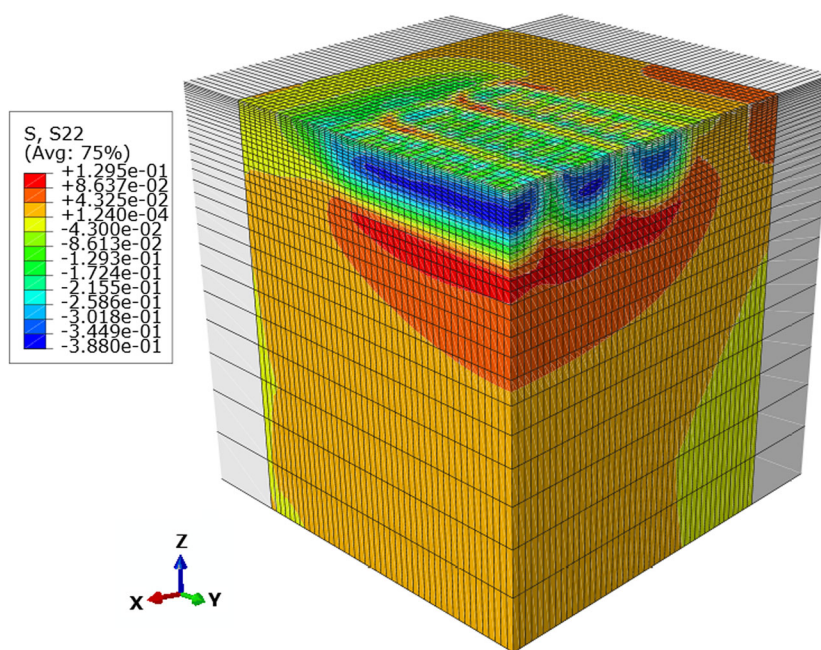


Fig. 7 Residual stress field within 1/4 model

It also can be seen from Fig. 10 that when the impact velocity varies from 1 to 2 m/s, the depth and the magnitude of maximum compressive residual stress increase with the impact velocities. When the impact velocity varies from 2 to 3 m/s, the maximum compressive residual stress decreases on the center line and increases on the offset line with the impact velocities, attributed to the increase of the surface coverage. With the increase of the impact velocities, the size of the impact indentation increases, and then the compressive residual stress zone increases. When the impact velocity is low, the compressive residual stress zone is small, which makes interaction between the adjacent indentations smaller. The compressive residual stress increases with the impact velocity. While the impact velocity is high, the interaction is large, in which the residual stress is similar to that described in Fig. 5. And the maximum compressive residual stress will decrease and the compressive residual stress will be more uniform.

4.2 Influence of Pin Diameter

During the UIT process, the energy transferred to the specimen can be varied by modifying the pin mass. The initial

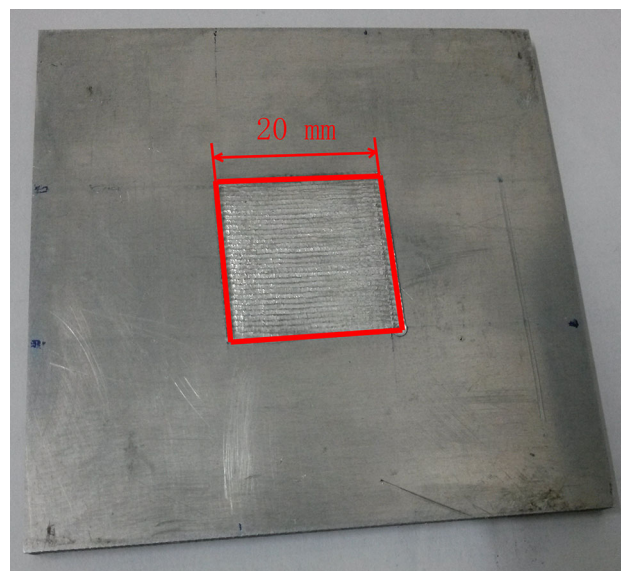


Fig. 8 Experimental results

velocity of the pin was 2 m/s and the pin tips had the same profile. Three different pin diameters (3, 4, and 5 mm) were selected to analyze the influence of pin diameter on the distributions of the residual stress, as shown in Fig. 11.

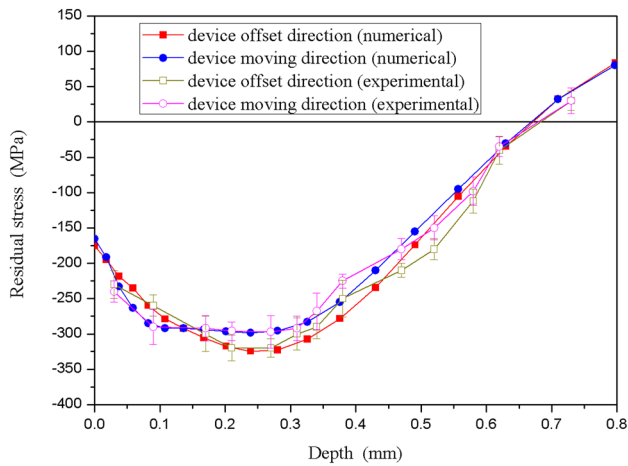
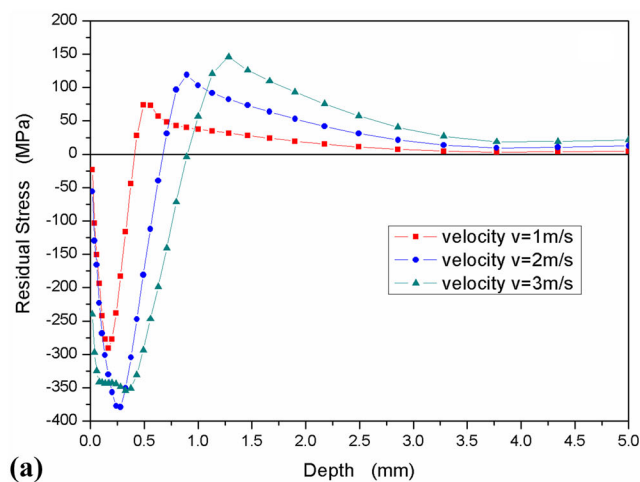
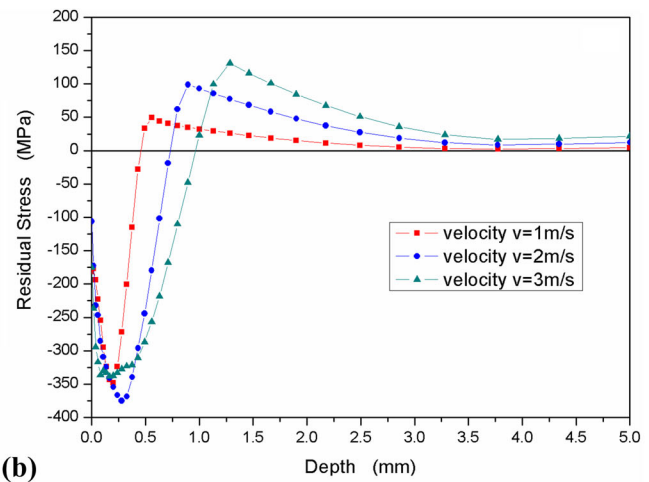


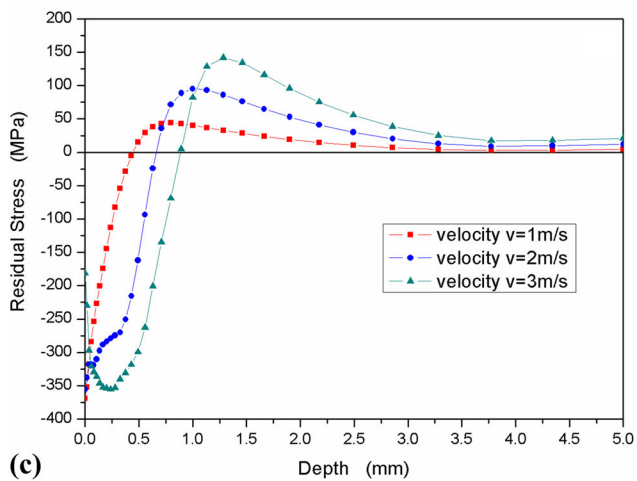
Fig. 9 Comparison of experimental and numerical results



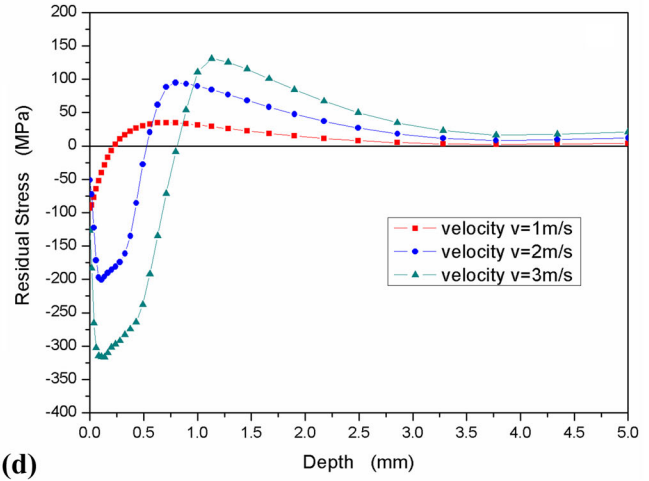
(a)



(b)



(c)



(d)

Fig. 10 Residual stress profiles with different initial impact velocities (a) in the offset direction along the center line, (b) in the device moving direction along the center line, (c) in the offset direction along the offset line, and (d) in the device moving direction along the offset line

Comparing with section 4.1, the similar results were obtained. When the pin diameter is low, the plastic zone induced by the impacts of each row is small, and the small overlapping of the plastic zone between the adjacent impact rows directly induced the maximum compressive residual stress at the specimen surface.

In order to compare the influences of the pin size and initial impact velocity on the residual stress distributions, the pin mass and initial impact velocity both increased by half. The relationship between the pin diameter and pin mass is

$$M = \rho(V_1 + V_2) = \rho \left[\frac{\pi D^2(L - b)}{4} + \frac{\pi D^2 b}{6} \right] = \rho \frac{\pi(3L - b)}{12} D^2, \quad (\text{Eq 4})$$

where ρ is the pin density, V_1 is the cylinder volume of the pin, V_2 is the semi-ellipsoid volume of the pin tip, D is the pin diameter, L is the pin length, and b is the length of the semi-axis. The pin diameter increased from 4 to 4.9 mm to increase the mass by half. And the initial impact velocity increased from 2 to 3 m/s. The comparison of results is shown in Table 3. The influence of pin diameter on the residual stress distribution is weaker than that of initial impact velocity.

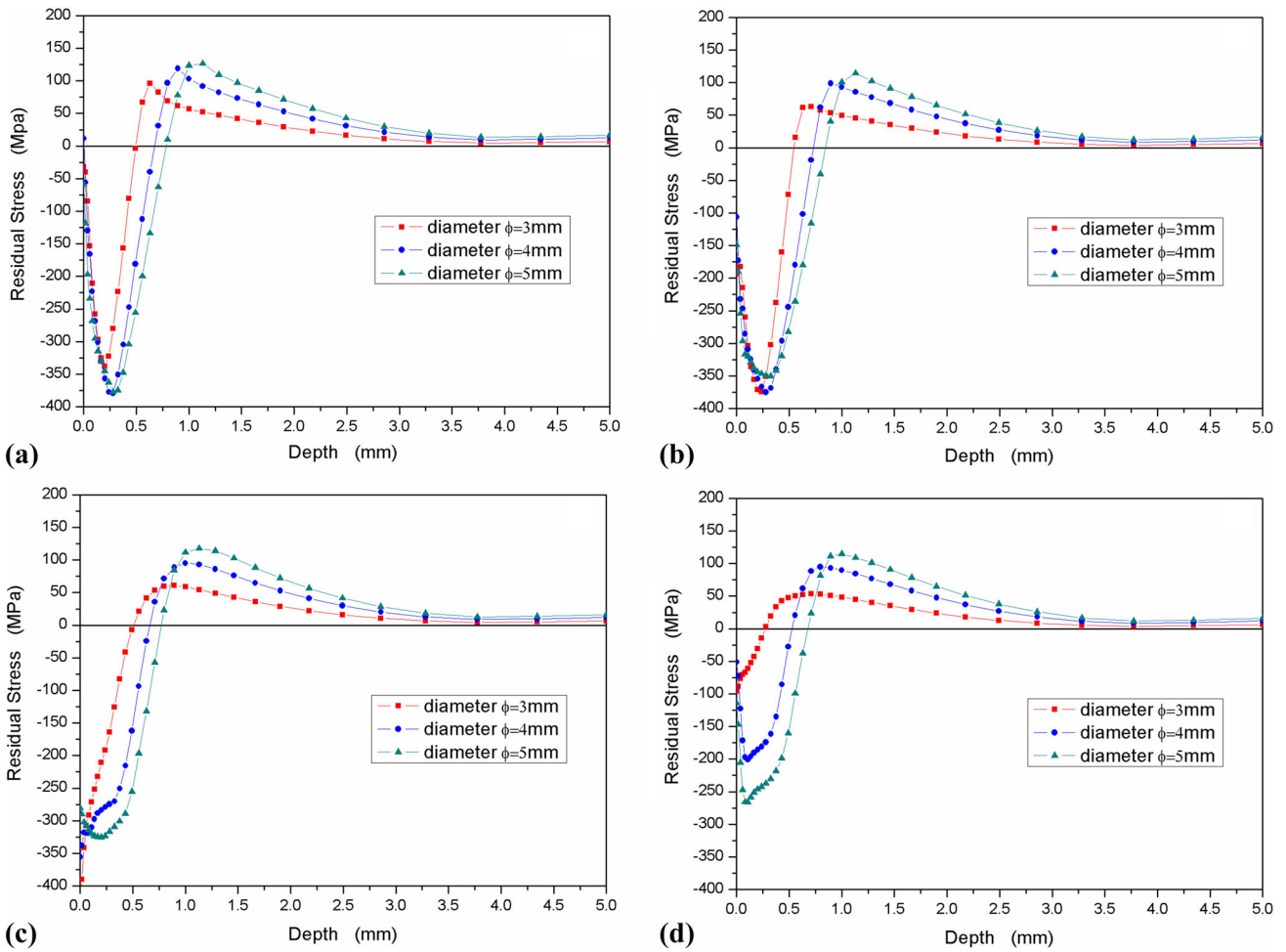


Fig. 11 Residual stress profiles with different pin diameters (a) in the offset direction along the center line, (b) in the device moving direction along the center line, (c) in the offset direction along the offset line, and (d) in the device moving direction along the offset line

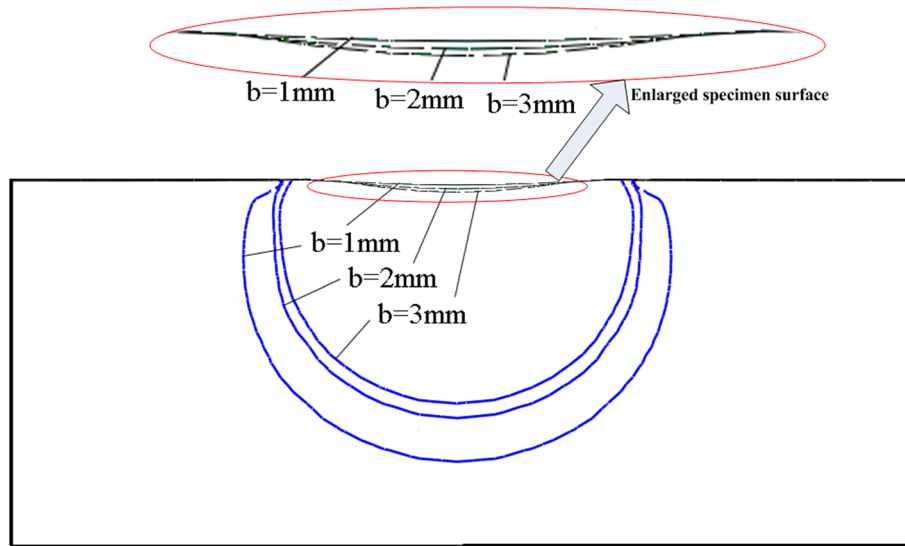


Fig. 12 Zone of plastic deformation with different pin tips

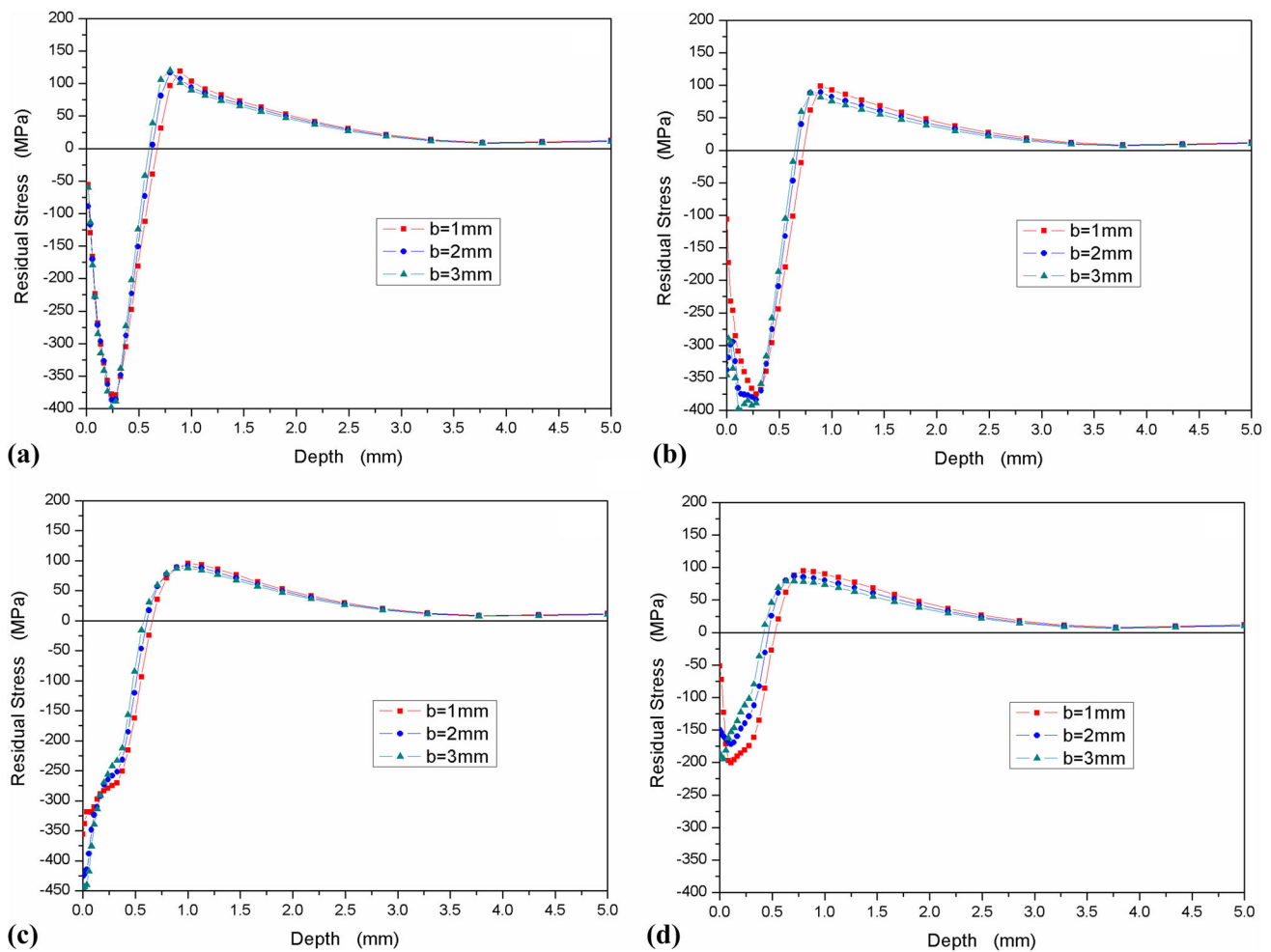


Fig. 13 Residual stress profiles with different pin tips (a) in the offset direction along the center line, (b) in the device moving direction along the center line, (c) in the offset direction along the offset line, and (d) in the device moving direction along the offset line

ties. It can be explained by the different kinetic energies of the impact pin for different controlled parameters, which would be transferred to the specimen.

4.3 Influence of Pin Tip

The pin tip is also a key parameter which is used to increase the impact intensity. The initial impact velocity was 2 m/s, pin diameter was 4 mm, and the pins had the same mass. Three different semi-axis b (1, 2, and 3 mm) values upon the residual stress distributions were analyzed. Figure 12 shows the size of the plastic deformation (the blue line) after single impact with different pin tips. With the increase of the semi-axis b , the indentation depth increases and the plastic zone decreases gradually. It also can be deduced that with the increase of the semi-axis, the contact areas between impact pin and specimen decrease, which induces the increase of energy density in the plastic zone transferred by impact. It can be seen from Fig. 13 that the increase of the energy density within the plastic zone could increase the maximum compressive residual stress, but due to the high surface coverage it increases slightly along the center line, especially in the offset direction. Due to the small indentation with large semi-axis, the edges of the impact rows cannot be overlapped in the offset direction, so the materials in the indentations are squeezed to the edge of the impact row, in

which large compressive residual stress is induced at the specimen surface, as shown in Fig. 13(c). Overall, the increases of the semi-axis cannot effectively influence the residual stress distributions.

4.4 Influence of Device Moving Velocity

In the UIT process, device moving velocity is one of the key parameters which could directly determine the surface coverage of the specimen in the device moving direction. Three different moving velocities were selected to analyze the distributions of the residual stress distribution. The relationship between the device moving velocity and the distance d_1 between the adjacent indentations are shown in Table 2, and the pin number (namely the impact number) used in each impact row was calculated separately. Fig. 14 shows the residual stress distributions along the center line and offset line. With the decrease of the device moving velocity, i.e., with the decrease of the distance d_1 between the adjacent impact locations, the penetration depth and the maximum compressive residual stress increase, but the increase is insignificant due to the stress-strain curve of the specimen. The center point of the specimen is impacted several times due to the high surface coverage in the device moving direction, but it is not easy to produce more plastic deformation because of the nonlinear stress-strain curve.

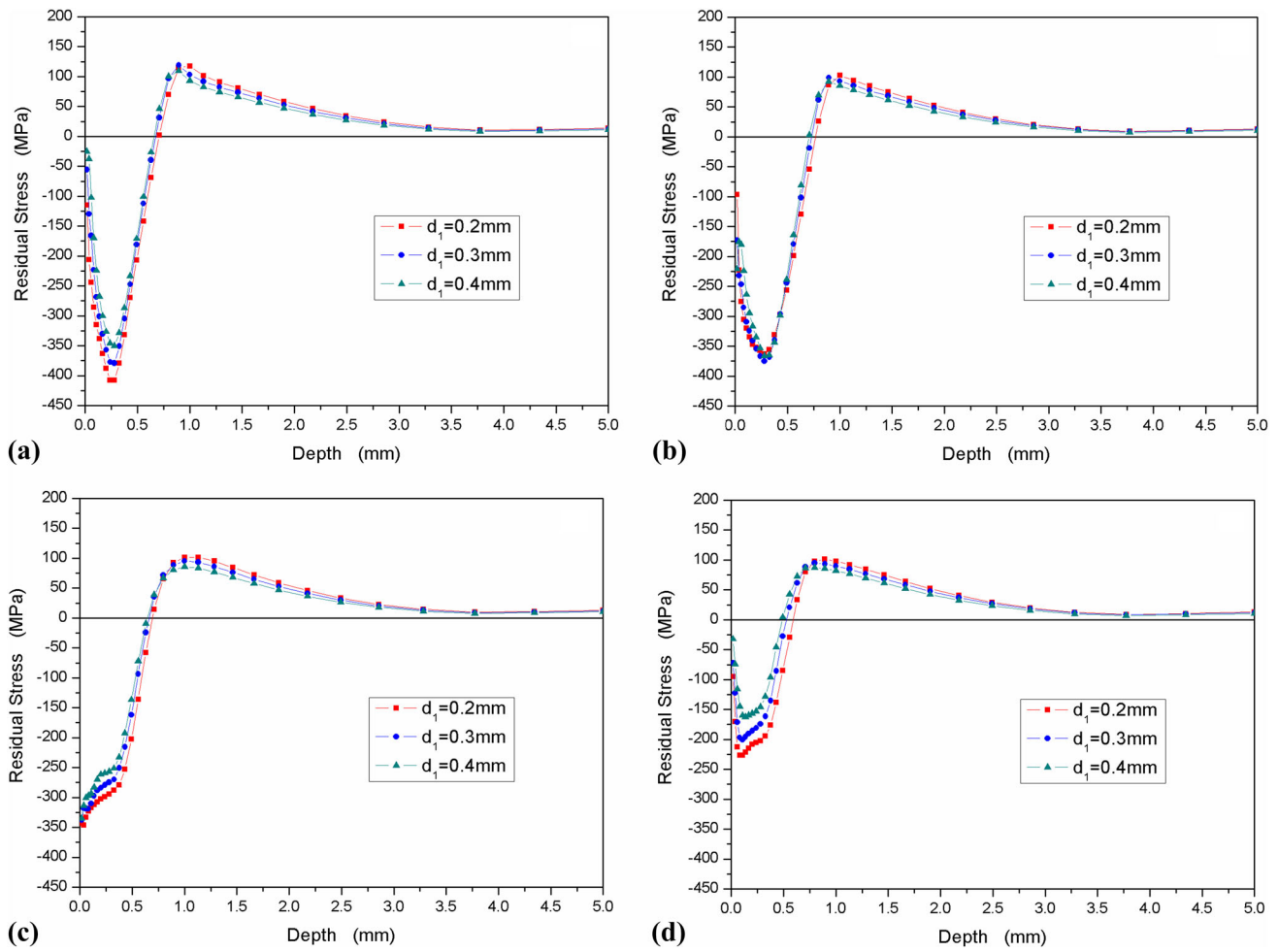


Fig. 14 Residual stress profiles with different distances d_1 (a) in the offset direction along the center line, (b) in the device moving direction along the center line, (c) in the offset direction along the offset line, and (d) in the device moving direction along the offset line

Thus, the residual stress along the center line changes slightly in the device moving direction. The surface coverage is low in the offset direction, the repeated impacts help enlarge the plastic deformation in this direction, and thus the maximum compressive residual stress would increase. According to Fig. 14(c), the maximum compressive residual stress appears at the specimen surface, which means that the indentations induced by the adjacent rows do not overlap. The decrease of the device moving velocity cannot increase the indentation diameter effectively.

4.5 Influence of Device Offset Distance

In the device offset direction, the coverage is relatively lower, and it could be adjusted using different device offset distances d_2 . In order to analyze the influence of different distances between the adjacent impact rows on residual stress, three different offset distances d_2 (0.5, 1, and 1.5 mm) were considered. Different impact row numbers were used and most of the impacts were restricted to the region of $4 \text{ mm} \times 4 \text{ mm}$. Fig. 15 shows the residual stress distribution along the center line and offset line of the specimen, and the offset distance is $\frac{d_2}{2}$ from the center line in the offset direction. When the distance d_2 is large (d_2 is 1 or 1.5 mm), the residual stress along the center

line changes slightly, which is attributed to the repeated impacts caused by the pin. Along the offset line, the residual stress is induced by the squeezing of the adjacent impact indentations, instead of by the impact directly. Therefore, when the distance d_2 is 1.5 mm, due to the squeezing of the adjacent indentations, the maximum compressive residual stress appears at the specimen surface. With the decrease of the offset distance, the squeeze within subsurface is decreased, which indicates that the compressive residual stress is lower when the distance d_2 is 1 mm, as shown in Fig. 15(c). When the distance d_2 is small (d_2 is 0.5 mm), the residual stress distribution can be explained by the theory described in section 3.1 with some exceptions. With the decrease of the distance d_2 , the maximum compressive residual stress decreases along the center line in the device moving direction, as shown in Fig. 15(b), and the plastic deformation and the residual stress distributions become more uniform, as shown in Fig. 15(c). But in the offset direction the maximum compressive stress increases with the decrease of distance d_2 , as shown in Fig. 15(a), which can be explained by the distance between the adjacent indentations in the device offset direction. Since the indentation distances in the offset direction are large, the interaction between the impacts of interval rows is weak, and the location of the maximum compressive residual stress does not change. With the decrease

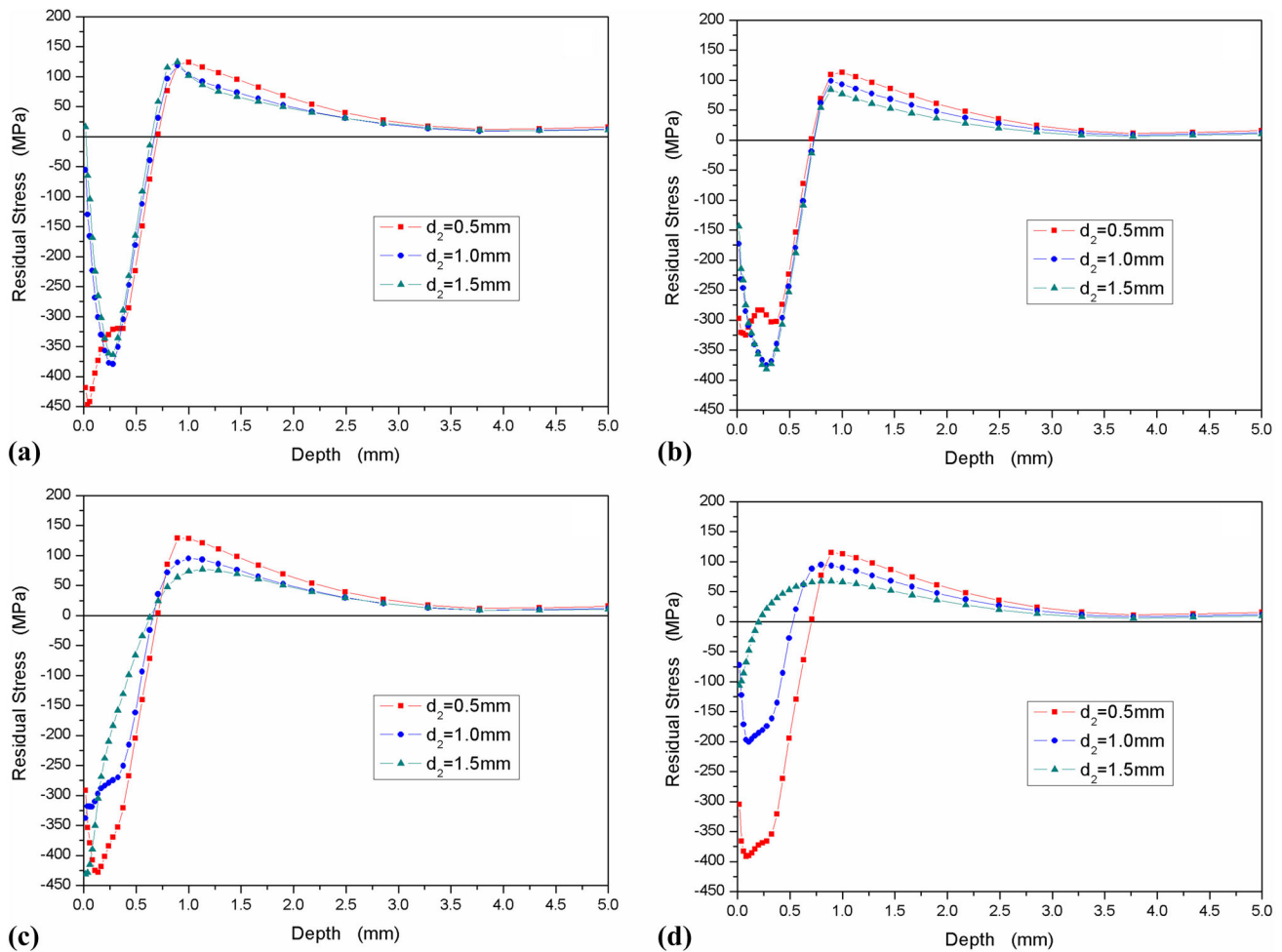


Fig. 15 Residual stress profiles with different distances d_2 (a) in the offset direction along the center line, (b) in the device moving direction along the center line, (c) in the offset direction along the offset line, and (d) in the device moving direction along the offset line

of d_2 , the maximum compressive residual stress increases and the uniformity of the residual stress is improved.

5. Conclusions

The multiple impacts on the 2024 aluminum alloy were modeled and simulated using ABAQUS/Explicit software. The influences of the controlled parameters on the residual stress distribution were examined and discussed. The following conclusions can be drawn:

- (1) The successive impacts during the UIT process will improve the uniformity of the plastic deformation and decrease the maximum compressive residual stress beneath the former impact indentations.
- (2) Due to the different surface coverage in different directions, the influences of the controlled parameters on the residual stress distributions are greater in the offset direction.
- (3) The influences of the controlled parameters on the residual stress distribution can be concluded as follows: (a) When the impact velocity and pin diameter are low, the depth and the magnitude of maximum com-

pressive residual stress increase with the increase of initial impact velocity or pin diameter; when the impact velocity and pin diameter are high, the depth and the magnitude of maximum compressive residual stress decrease on the center line and increase on the offset line. (b) The indentation depth increases and the plastic deformation decreases with the increase of semi-axis of the impact pin. (c) The penetration depth and the maximum compressive residual stress increase with the decrease of the distance between the adjacent impact locations, but the change is small, especially in the device moving direction. (d) When the device offset distance decreases from 1.5 to 1 mm, the residual stress along the center line changes slightly. When the distance d_2 decreases from 1 mm to 0.5 mm, the maximum compressive residual stress decreases along the center line in the device moving direction and increases in the device offset direction.

Acknowledgments

This work was supported by the National Natural Science Foundation of China (Grant No. 51275343).

References

1. X. Yang, J. Zhou, and X. Ling, Study on Plastic Damage of AISI, 304 Stainless Steel Induced by Ultrasonic Impact Treatment, *Mater. Des.*, 2012, **36**, p 477–481
2. G. Liu, J. Lu, and K. Lu, Surface Nanocrystallization of 316L Stainless Steel Induced by Ultrasonic Shot Peening, *Mater. Sci. Eng. A Struct.*, 2000, **286**, p 91–95
3. X. Cheng, J.W. Fisher, H.J. Prask, T. Gnäupel-Herold, B.T. Yen, and S. Roy, Residual Stress Modification by Post-Weld Treatment and its Beneficial Effect on Fatigue Strength of Welded Structures, *Int. J. Fatigue*, 2003, **25**, p 1259–1269
4. Y.F. Al-Obaid, Three-Dimensional Dynamic Finite Element Analysis for Shot-Peening Mechanics, *Comput. Struct.*, 1990, **36**, p 681–689
5. K.I. Mori, K. Osakada, and N. Matsuoka, Finite Element Analysis of Peening Process with Plasticity Deforming Shot, *J. Mater. Sci. Technol.*, 1994, **45**, p 607–612
6. S.A. Meguid, G. Shagal, and J.C. Stranart, 3D FE Analysis of Peening of Strain-Rate Sensitive Materials Using Multiple Impingement Model, *Int. J. Impact. Eng.*, 2002, **27**, p 119–134
7. K. Schiffner and C.D.G. Helling, Simulation of Residual Stresses by Shot Peening, *Comput. Struct.*, 1999, **72**, p 329–340
8. A. Ebenau, O. Vohringer, and E. Macherauch, Influence of the Shot Peening Angle on the Condition of Near Surface Layers in Materials, *Proc. ICSP*, 1987, **3**, p 253–260
9. S.T.S. Al-Hassani, K. Kormi, and D.C. Webb, Numerical Simulation of Multiple Shot Impact, *Proc. ICSP*, 1999, **7**, p 217–227
10. J. Schwarzer, V. Schulze, and O. Vöringer, Evaluation of the Influence of Shot Peening Parameters on Residual Stress Profiles Using Finite Element Simulation, *Mater. Sci. Forum*, 2003, **395**, p 1–6
11. T. Hong, J.Y. Ooi, and B.A. Shaw, A Numerical Study of the Residual Stress Pattern from Single Shot Impacting on a Metallic Component, *Adv. Eng. Softw.*, 2008, **39**, p 743–756
12. G.H. Majzoobi, R. Azizi, and A.A. Nia, A Three-Dimensional Simulation of Shot Peening Process using Multiple Shot Impacts, *J. Mater. Process. Technol.*, 2005, **164–165**, p 1226–1234
13. S. Bagherifard, R. Ghelichi, and M. Guagliano, A Numerical Model of Severe Shot Peening (SSP) to Predict the Generation of a Nanostructured Surface Layer of Material, *Surf. Coat. Technol.*, 2010, **204**, p 4081–4090
14. M. Klemen, V. Schulze, I. Rohr, and D. Löhe, Application of the FEM for the Prediction of the Surface Layer Characteristics After Shot Peening, *J. Mater. Process. Technol.*, 2009, **209**, p 4093–4102
15. T. Chaise, J. Li, D. Nélias, R. Kubler, S. Taheri, G. Douchet, V. Robin, and P. Gilles, Modelling of Multiple Impacts for the Prediction of Distortions and Residual Stresses Induced by Ultrasonic Shot Peening (USP), *J. Mater. Process. Technol.*, 2012, **212**, p 2080–2090
16. C. Guo, Z. Wang, D. Wang, and S. Hu, Numerical Analysis of the Residual Stress in Ultrasonic Impact Treatment Process with Single-Impact and Two-Impact Models, *Appl. Surf. Sci.*, 2015, **347**, p 596–601
17. C. Guo, S. Hu, D. Wang, and Z. Wang, Finite Element Analysis of the Effect of the Controlled Parameters on Plate Forming Induced by Ultrasonic Impact Forming (UIF) Process, *Appl. Surf. Sci.*, 2015, **353**, p 382–390
18. G. Kay. Failure Modeling of Titanium-61-4 V and 2024-T3 Aluminum with the Johnson-Cook Material Model. Final Report-U.S. Department of Transportation: Federal Aviation Administration, FAA Report No. DOT/FAA/AR-03/57, 2003